Annual flood damages influenced by El-Niño in Kan River Basin, Iran

Farhad Hooshyaripor[1], Sanaz Faraji-Ashkavar[2], Farshad Koohyian[1], Qiuhong Tang[3,4*], Roohollah Noori[5]

[1]Department of Civil Engineering, Architecture and Art, Science and Research Branch, Islamic Azad University, Tehran, 1477893855, Iran
[2]Department of Civil Engineering, Al-Taha University, Tehran, 1488836164, Iran
[3]Key Laboratory of Water Cycle and Related Land Surface Processes, Institute of Geographic Sciences and Natural Resources Research, Chinese Academy of Sciences, Beijing, 100101, China
[4]University of Chinese Academy of Sciences, Beijing, 100049, China
[5]School of Environment, College of Engineering, University of Tehran, Tehran, 141785311, Iran

Correspondence to: Qiuhong Tang (tangqh@igsnrr.ac.cn)

Abstract. Although many studies have explored the effect of teleconnection patterns on flood, few investigations have focused on the assessment of expected flood damages under such large-scale atmospheric signals. This study aims at determining the effect of the most emblematic teleconnection, El-Niño, on the expected damages due to floods with low return periods in Kan River basin, Iran. To determine the flood damage costs, median of annual precipitation changes (ΔP) during El-Niño condition was used, although ΔP cannot necessarily be transferred to extreme values. Then, the flooded area was determined under the increased rainfall due to El-Niño for 5-, 10- and 50-year return period. The results showed that El-Niño has increased the annual precipitation by 12.2%. Flood damage assessment using damage-depth curves showed that the relative increase of expected damage during El-Niño condition is much higher for short return period floods than that for long return period floods. In general, 12.2% increase in the annual precipitation would increase the damage by 1671% and 176% respectively for the return periods of 5- and 10- year. However, in the case of 50-year flood this increased percentile reduced to 52%. These results indicate the importance of small flood events in flood management planning during El-Niño.

1 Introduction

In recent decades, frequency of flood events and the resultant damages have been increasing dramatically in Iran. According to the available reports, the number of flood events in Tehran over four decades had grown from 12 cases in 1951 to 54 cases in 1991 (Farsnews 2015; Saghafian et al. 2017). Climate change, approaching to floodplain, land use changes, diversion of the waterways, destructive effects of human activities, degradation of forests and pastures, construction of dysfunctional and vulnerable hydraulic structures can be mentioned as the reasons for increasing flood risks (Wang et al. 2019; Tang 2020). The magnitude and frequency of flood events in each region depends on several factors: (i) physiographical features of the catchment such as shape, slope, and rivers network density, (ii) hydrological features such as precipitation, storage and initial losses, evapotranspiration, and permeability, (iii) human activities, (iv) large-scale atmospheric signals and (v) climate change (Noori et al. 2011; Ward et al. 2014; Alizadeh-Choobari and Najafi 2017; Hooshyaripor and Yazdi 2017; Hooshyaripor et al.

2017; Saghafian et al. 2017; Hao et al. 2018). These factors affect the frequency and intensity of flood and consequently the amount of damage costs. Identifying these factors will help to manage the flood and reduce the risks. In recent years, the effects of teleconnection phenomena on regional climate have been increasingly discussed. Prediction of teleconnection indicators helps to reduce the flood damages by implementing the necessary practical measures (Schöngart and Junk 2007). Sun et al. (2015) showed that parts of North and South America, South and East Asia, South Africa, Australia and Europe are affected by El-Niño Southern Oscillation (ENSO). Schöngart and Junk (2007) showed that there is a strong correlation between ENSO and Amazon River flood such that the river water level decreases in the warm episode of the ENSO (El-Niño) and increases in its cold episode (La-Niña). Grieco and DeGaetano (2018) concluded that the occurrence of El-Niño in the winter reduces the frequency of high waves in the east of the Ontario Lake, while there was no meaningful relationship in the conditions of La-Niña. Azmoodehfar and Azarmsa (2013) showed that the southeast of Iran during the years with the event of La-Niña experienced a higher-than-normal maximum and minimum temperature. In a global study, Ward et al. (2014) investigated the impact of ENSO on the daily peak discharge of some important rivers and showed that ENSO exerts strong and widespread influences on both flood hazard and risk. Saghafian et al. (2017) showed that in the Dez and Karoun basins (located in the west and southwest of Iran) during March and April the El-Niño increases maximum annual flood and vice versa in the case of La-Niña. Their results showed that the maximum annual flood during El-Niño events is much greater than that during La-Niña events. Gholizadeh (2015) investigated the effect of El-Niño on the rainfall events between 1973 and 2012 and concluded that the El-Niño phenomenon increases the annual rainfall of Iran. Hooshyaripor et al. (2019) investigated the impact of different teleconnection indices on Iran rainfall, and concluded that El-Niño can enhance the annual precipitation by nearly 40%. They stated that due to the increase of rainfall, the river discharge would be affected directly. So far, many studies have focused on the impact of El-Niño over river flow. Alizadeh-Choobari and Najafi (2017) indicated that the ENSO cycle contributes to the interannual climate variability over Iran. According to their results, about 26% of the variance in annual precipitation over Iran is related to the El-Niño. Based on their achievements, in spite of the seasonality of the ENSO signal and its interannual variability, Iran is anomalously wet during El-Niño and dry during La Niña and the impacts of La Niña and El-Niño are generally stronger over the warm and arid regions.

Although, the effect of ENSO on the precipitation has been frequently studied, there are few studies about ENSO influence on the socioeconomic damages and losses of floods (Ward et al. 2014). The main reason for the limited research on the economic impacts of climate and hydrologic variability is the lack of economic data on flood damages (Changnon 2003). Analyzing the National Flood Insurance Program daily claims and losses and Multivariate ENSO Index (MEI), Corringham and Cayan (2019) quantified insured flood losses across the western United States from 1978 to 2017. They showed that in coastal Southern California and across the Southwest of the United States, El-Niño has had a strong effect in producing more frequent and higher magnitude of insured losses, while in the Pacific Northwest, the opposite pattern with less insured losses has been reported. Changnon (2003) revealed that the strong El-Niño events of 1982/83 and 1997/98 have caused significant flood damages over $2.8 billion in Southern California. Null (2014) demonstrated that from 1949 until 1997 out of the six seasons that flood damages costs exceeded $1 billion in California, the year of three cases had been El-Niño years with one very strong

(1982), one moderate (1994) and one weak (1968) El-Niño year. Ward et al. (2014) assessed ENSO's influence in terms of affected population, gross domestic product and economic damages caused by flood risk at the global scale and showed that climate variability, especially from ENSO, should be incorporated into disaster-risk analyses and policies. They revealed that, if the frequency and/or magnitude of ENSO events were to change in the future due to climate change, change in flood-risk variations across almost half of the world's terrestrial regions would occur. Ward et al. (2016) provided a global modelling exercise to examine the relationships between flood duration and frequency and ENSO. They indicated that the duration of flooding compared to flood frequency is more sensitive to ENSO.

The above studies indicate the importance of teleconnection on the flood characteristics in many parts of the world, although few investigations have focused on the assessment of the expected damages under the El-Niño or La-Niña conditions. Obviously, damage assessment is an important part of flood risk analysis, which determines the need for flood management programs and their priorities. The question addressed in this research is that, given the increasing impact of rainfall due to El-Niño, how much damages are expected to be added in a given study area. To answer this question, the catchment of Kan River in north of Tehran metropolis was selected and a simplistic approach was employed to estimate the flooding area and the damages. Due to importance of the basin, numerous flood risk studies have been conducted in this area (WRI 2011a,b,c; Yazdi and Salehi Neyshabouri 2012; Yazdi et al. 2013). Hence, this paper focuses on the impact of El-Niño not only on the precipitation amount but also on the flood damages that are expected to be increased during El-Niño condition.

2 Study area

The Kan River basin is one of the most important basins located in the north of Tehran city and a flood vulnerable area (Yazdi and Salehi Neyshabouri 2012). It is reported that in the flood of July 15, 2015 a 20-minute storm caused 8 losses of life, several bridge and diversion dam failures, and more than 10 million dollars in damages to the residential, commercial and agricultural areas (ISNA 2015). In June 1968 a heavy rain as 6 times as the mean annual precipitation happened in 2 days caused 31 losses of life and huge damages to the properties. In general, during a period of 60-year (from 1954 to 2015) at least 8 flood events that resulted in loss of life (in total 2200 people) had been reported in Kan River basin and central Tehran areas. Existence of many restaurants, demographic, recreational, tourist and pilgrimage centres adjacent to the sloping Kan River have exacerbated the potential for damages (WRI 2011a).

The Kan River Basin is located between the longitude of the 51º 10' and the 51º 23' and the latitude of 35º 45' to 35º 58'. The basin can be divided into 10 sub-basins (Figure 1). The highest point of the basin is 3823 m and the lowest point is 1328 m with the average of 2377 m above sea level. The area of the basin is 216 km^2. The average annual precipitation is 640 mm and the average annual discharge is 78.23 Mm^3 at Sulaghan station. The hydrometric stations include Kiga (Gauge1), Keshar (Gauge2) and Sulaghan (Gauge3) (Figure 1). As shown in Figure 1, there are three rain gauge stations in the basin and four synoptic stations around the basin.

3 Methodology and data

In this study, teleconnection indices namely southern oscillation index (SOI), Multivariate ENSO Index (MEI), Arctic Oscillation (AO), North Atlantic Oscillation (NAO), and Madden Julian Oscillation (MJO) were evaluated. An index that has the highest correlation with the precipitation in the study area were selected for further analysis. The Fisher's exact test of independence was used to test the significance of correlation between the teleconnection indices and precipitation. In the Fisher's exact test the null hypothesis is that "two variables are independent". In other words, the relative proportions of each teleconnection index are independent of the precipitation:

$$H_0 : \rho = 0$$
$$H_1 : \rho \neq 0 \quad (1)$$

Considering the Fisher's exact test, if p-value is less than 0.05 the null hypothesis is rejected; i.e. the p-value must be less than 0.05. According to the results (Table 1), there would be a statistically significant association between the SOI (MEI and NAO, as well) and precipitation. However, SOI has the highest correlation with the precipitation in the Kan River basin. Therefore, ENSO is the most important large-scale atmospheric signal that affects precipitation in the Kan River basin. It has been shown that rainfall intensity increases in the conditions of El-Niño and decreases in the conditions of La-Niña. Accordingly, the present study will assess the increase in flood damage due to El-Niño occurrence. For this purpose, the following steps have been taken.

Step I: Estimating the lag time (T_l) between the El-Niño event and the precipitation in the study area. As the effect of ENSO takes time to be experienced in far geographic locations, the lag time between the ENSO occurrence and the related influences in Kan River Basin was firstly calculated. This lag time can be estimated by comparing the variations of SOI with local precipitation time series. The monthly rainfall at the nearby synoptic stations including Mehrabad (1951-2017), Shemiran (1988-2017), Tehran-Geophysics (1992-2017) and Chitgar (1997-2017) (See Figure 1) and monthly SOI values are used. A statistical method, average mutual information (AMI), is used to determine the time delay. This method is based on the Shannon entropy theory and is a measure of "amount of information" obtained about one random variable, through the other random variable. Guiasu (1977) defined the mutual information of two random variables as a measure of the mutual dependence between two variables. Not limited to real-valued random variables and linear dependence like the correlation coefficient, mutual information is more general and determines how different the joint distribution of the pair (X,Y) is to the product of the marginal distributions of X and Y (Guiasu 1977). Suppose A is monthly precipitation in the representative station of the basin and B is SOI. The AMI is defined between two measurements a_i and b_i belonging respectively to the sets A and B as follows (Cover and Thomas 1991):

$$I_{AB} = \sum_{i=1}^{K}\sum_{j=1}^{K} P_{AB}\left(a_i, b_j\right)\log\left(\frac{P_{AB}\left(a_i, b_j\right)}{P_A\left(a_i\right)P_B\left(b_j\right)}\right) \quad (2)$$

where $P_{AB}(a_i, b_j)$ is the conjugate probability density for measurements A and B with values of a and b, respectively; $P_A(a_i)$ and $P_B(b_j)$ are the probability density function for measurements A and B. If a_i (the measurements of A) is independent of b_i (the measurements of B) then the value of I_{AB} will be zero. In this paper, probabilities P_A and P_B were calculated using empirical frequency analysis in which the relative frequency histograms for both time series, SOI and precipitation were determined. The values of AMI of different arbitrary lag-times (1 to 12 months) between SOI and precipitation were calculated. The higher AMI value, the more dependency between two time series. Therefore, that lag-time corresponding to the highest AMI value was selected as the lag-time between the time series. This method determines the lag time between two time series by using the nature of the data itself without any predetermined format based on probabilistic concepts (Cover and Thomas 1991). In Eq. (2), K is the optimal number of statistical categories for fitting the statistical distribution on the measurements A and B. When dealing with large sets of numbers, Sturge's rule (Sturges 1926) can be used to choose the number of categories. Sturge's rule is widely used in the statistical packages like excel for making histograms. According to Sturge's rule the data range should be split into K equally spaced classes where:

$$K = 1 + 3.332 \log_{10}(n) \quad (3)$$

where n is the number of data in the corresponding interval (here n = 480); therefore, in the present study, K = 10. Noted that there is uncertainty in the optimal number of categories that may influence the lag time between the precipitation in the basin and SOI.

Step II: Estimating the amount of rainfall variation under the influence of El-Niño. Secondly, the influence of El-Niño on the precipitation amount in Kan River Basin is quantified. The influence is estimated using a statistical method by calculating the expected value of the changes of precipitation amount in the El-Niño episodes compared to those in the neutral periods. In this study the SOI values were obtained from National Oceanic and Atmospheric Administration (NOAA) website (https://www.cpc.ncep.noaa.gov/data/indices/soi). Prolonged periods of negative SOI values accompany the abnormally warm ocean waters across the eastern tropical Pacific. La-Niña and El-Niño are characterized respectively by SOI>+1 and SOI<-1 (WRCC, 2010). Then, annual precipitation change (PC) in the El-Niño condition is calculated as follow:

$$PC_t = \left(P_{El\,t} - P_N\right)/P_N \quad \forall t = 1...T \quad (4)$$

where $P_{El\,t}$ (mm) is annual rainfall in every El-Niño episode; P_N (mm) is average annual rainfall in the normal episodes; and T is number of El-Niño events in the time period (here T=6). Then, the median of PC values (ΔP, mm) will be used to construct synthesized rainfall storms. It should be noted that one limitation of this research is that the annual change factor is applied in the extreme rainfalls of short time scales. Certainly, it is better to consider the monthly or seasonal change factor or to use extreme rainfalls on the basis of recorded storms. However this paper uses annual precipitation and a change factor to estimate extreme rainfall due to data limitation.

Step III. Estimation of design rainfalls with different return periods. Thirdly, several design storms are generated. The rainfall storms are synthesized based upon the average precipitation change during El-Niño events. The designed storms are used for

assessing the flood damages in a certain return period. To do so, the intensity-duration-frequency (IDF) rainfall curve of Kan basin was obtained from WRI (2011b). Time of concentration (T_c) of the basin is 135.19 min (Using Kirpich equation). Therefore, the intensity of design rainfall (i_d) can be deduced for different return periods (here, three return periods of 5-yr, 10-yr and 50-yr are considered). These return periods are selected in accordance with the paper's objective to show the importance of small floods in flood management plans compared to the high return period floods. Then, the rainfall intensity in the El-Niño condition (i_E) can be calculated by multiplying i_d and ΔP.

Step IV: Hydrological modeling. Fourthly, the HEC-HMS hydrologic model is used to simulate the rainfall-runoff process using the design storms generated in Step III. The hydrologic model is run for each return period. The simulated peak discharge is used in the next step to estimate the flooding depth. In the hydrologic model, the SCS method is used to calculate the effective rainfall (P_e, mm):

$$P_e = \frac{(P - 0.2S)^2}{P + 0.8S} \quad (5)$$

where P (mm) is rainfall; and S (mm) is potential maximum retention. The constant value 0.2 is selected based on SCS recommendation to estimate initial losses as I_a=0.2S (Ponce and Hawkins 1996). Moreover, Clark instantaneous unit hydrograph method is applied to transform the effective rainfall into runoff (Q) and two-parameter Muskingum method is used for flood routing. The Muskingum method calculates the discharge within the river given the inflow hydrograph at the upstream end. For calibration of the HEC-HMS model, hourly historical storms which had been recorded in three rain gauge stations in the basin and the related runoffs at the hydrometric stations (Figure 1) are used. Noted that for calculation of rainfall specified to every sub-basin, the gauge weight method is used where the weights were determined from Thiessen method. The curve numbers (CN) and time of concentrations (T_c) are calibrated within 10 sub-basins. For calibration and verification of the hydrologic model four storm events were extracted from 15 years available data (2000-2014): 1) the storm of 15–18 April 2003 in which a flood of maximum 38.22 m^3/s was recorded at Gauge3; 2) the storm of 16–19 April 2002 where the peak discharge rate of 32.3 m^3/s was recorded at Gauge3; 3) the storm of 15–17 April 2009 in which a flood of maximum 34 m^3/s was recorded at Gauge3; and 4) the storm of 11–13 March 2011 where the peak discharge rate of 55.1 m3/s was recorded at Gauge3. Then the calibrated model can be used for modelling the rainfall of given return periods to calculate the flood hydrographs at the outlet of the sub-basins.

Step V: Hydraulic modeling: Fifthly, the HEC-RAS model is used for hydraulic modeling and determination of flood depth at the target points (Residential areas shown in Figure 1). Based on the obtained flood depth, the flooding area is determined for designed storms in the El-Niño and neutral episodes. HEC-RAS is a one-dimensional model based on the numerical solution of the Saint-Venant equations. The model is calibrated by adjusting the Manning roughness coefficients at different river sections. The calibrated HEC-RAS model under steady state condition is then driven by the simulated peak discharges from HEC-HMS hydrologic model to simulate flood depths at the target points.

Step VI. Estimating expected damage cost. Finally, flood damage is assessed for all 6 runs of the model. These damages can be compared to each other in order to determine the role of El-Nino on the flood damages. Damage caused by flooding can be divided into two groups: tangible and intangible damages. Intangible damages are those caused by illnesses and mental problems due to loss of life or properties. Tangible damage can be categorized into two direct and indirect damages. Direct damage is that caused from flooding of the buildings and properties such as home equipment, crops, livestock and poultry. Indirect damages are those caused due to disruption of trade and business, threating life and needs to emergency services, and so on. Noted that, this paper focuses on the direct tangible damages only.

Damage caused by flood is a function of its characteristics, including flow depth and inundation amount, duration of inundation, and flow velocity. One of the commonly used methods for estimating flood damages is damage-depth curve method which gives the relationship between damage percentile and flood depth (Corry et al. 1980, KGS_Group 2000, Messner et al. 2007; Olesen et al. 2017; Wobus et al. 2017; Jamali et l. 2018). The damage-elevation curves are prepared for different land uses of Kan River Basin (Figure 2) by the Federal Emergency Management Administration (Berkman and Brown 2015). The main land uses of the Kan River floodplain are residential buildings, restaurants, and fruit gardens (WRI 2011c). The damage cost is then calculated to include the total monetary value of the inundated land use-specific property. A comprehensive analysis of physical damages due to flooding requires information including accurate land use map, area and age of buildings, type of structures, number of floors, exact area of different agricultural crops in the flood-prone area, crop number per unit area, value of crops, value of buildings and their contents, number of residential, administrative, and commercial buildings in the flood prone areas, area and elevation of buildings, their locations, and spatial distribution of flood depth in the inundated areas for different return periods. In this paper a simplistic approach is used for this regard. For the building damage analysis, separating buildings into residential and commercial ones, the total area of inundated buildings, average inundation depth, and the average economic value of the buildings and their contents for every building type are considered. For agricultural damage analysis, considering the dominant crops of cherry and apple, the area of inundation, average inundation depth, crop density, and average price of one single crop, the flood damage is assessed.

4 Results and discussion

Monthly analyses of the precipitation in the synoptic stations and SOI using AMI method showed that there is no lag time between rainfall and SOI time series (the lag time is less than one month). There are 161 months with El-Niño and 128 months with La-Niña over the period of 1951-2017. The average monthly rainfall at Mehrabad station in the El-Niño episodes is 21.4 mm and in the La-Niña episodes is 16.2mm, while in the normal episodes it is 19 mm. In Figure 3, the annual rainfall of stations is plotted against the SOI index. It is obvious that with decreasing SOI index, annual rainfall increases in the study area and vice versa. In the period of 1951-2017, a total of 6 El-Niño (SOI<-1) and 5 La-Niña (SOI>+1) events have been occurred. Out of the 6 El-Niño years, 5 periods have experienced increase in the precipitation (2%-45%) and 1 period with decrease in the precipitation (-34%). The largest event for El-Niño dates back to 1983 and 1987 with respectively 334 mm and

252 mm recorded rainfall in Mehrabad station. Furthermore, based on the trendlines, one unit decrease in SOI would lead to 22.5 mm increase of annual rainfall at Mehrabad station (Figure 3a). For further analyses, Mehrabad station was chosen because it has more data than the other stations. There are 6 years with El-Niño and 55 normal years among the total of 66 years (1951-2017). Using Eq. (4), for the 6 years with El-Niño condition, the *PC* values range from -34% to 45% while the latter is related to the year 1983 in which a high value of 334 mm rainfall was recorded. The median of the *PC* values can be calculated (ΔP=12.2%). It should be noted that, the threshold of SOI=-1 is an assumption that affects the results significantly. The Kan River Basin has 135.19 min time of concentration. Therefore, considering the duration of the design rainfall as D=150 min, i_d can be estimated from IDF curves. For return periods of 5, 10, and 50-yr, i_d values are 7.8, 9.5, and 13 mm/hr, respectively. Thus, i_E values can be calculated as 8.76, 10.66, and 14.59 mm/hr respectively for return periods of 5, 10, and 50-yr.

4.1 Hydrologic and hydraulic modeling

The HEC-HMS model was calibrated using a flood event recorded in April 2003. The calibration parameters include curve number (CN) and concentration time (T_c) of the sub-basins. In the process of automatic calibration, the parameters are determined such a way that the model could simulate the hydrologic behaviour of the basin accurately. The main objective is to predict the exact peak discharge and time to peak of the hydrograph in the hydrometric stations by minimizing the mean squared error (MSE) between predictions and observations. Figure 4a shows the comparison between the observed and simulated hydrographs in Gauge3. Figure 4b shows the results for the upstream gauges (Gauge1 and Gauge2). Table 2 shows the calibrated parameter values for the hydrologic modeling. The hydrologic model is verified with the flood events in April 2002, April 2009 and March 2011 which are with respectively peak discharges of 31.5 m^3/s, 34.4 m^3/s and 54.1 m^3/s. Comparison between the simulated and observed flood hydrographs are shown in Figure 4c. It is noted that, for the flood in March 2011, the peak value of 54.1 m^3/s was provided by the estimation of Regional Water Company of Tehran. The discharges in the upstream stations are not available and thus are not compared. The verification suggests that the model using the estimated parameters can be used to predict flood hydrographs under the design storms at the sub-basins.

Then HEC-RAS model is used to simulate the flood travelling and to determine the flood depths of different return periods in the target points. For starting the hydraulic modelling, HEC-RAS requires cross sections of the river in different points. In this study the cross sections were extracted from Digital Elevation Model. Flood hydrographs of the sub-basins with different return periods were simulated by the calibrated rainfall-runoff model (HEC-HMS) and the peak values were used as the boundary conditions for the HEC-RAS model. For the model's calibration, the peak discharges produced in the hydrologic model's calibration step (the flood event during 15–18 April 2003) are input into the hydraulic model as the boundary conditions at the upstream reaches and the flood depth and discharge at Sulaghan station are compared with the observations. The parameters of the HEC-RAS model such as Manning roughness coefficients are calibrated manually. For the model

verification, the flood event of 16–19 April 2002 and the upstream peak discharges generated by the hydrologic model are used.

The hydrologic and hydraulic models are applied for modelling floods under the design storms of 5-, 10-, and 50-year return periods. For flood under design storms of each return period, one model run under El-Niño and one under normal condition are required. There are total 6 different runs of the combined hydrologic and hydraulic modeling. Using the obtained inundated depths, the flood mapping can be shown. Figure 5 illustrates the inundation areas at two target points (Sulaghan and Sangan villages) for the 50-yr flood in the normal condition.

4.2 Damage analysis

In this section, with the help of GIS tool and the land use maps (generated from maps of 1/25000 scale) which were obtained from the local municipality, the results of a simple analysis of flood damages are provided. Only five sub-basins, namely Imamzadeh Davood, Rendan, Sangan, Sulaghan and Keshar, are considered because of lack of data in the other sub-basins. As noted previously, here a simplistic approach with several limitations is used. The main reason is lack of precise land use information and accurate monetary value of property in the basin.

The flood damage to each land use type is assessed using the average economic value of one unit of that land use. It should be noted that for agricultural physical damages analysis in each sub-basin, two dominant products of cherry and apple were identified, and the average crop number per unit area and value of each crop were used to calculate total flood damage based on the areal percentage of each crop type. The percentages of crops, number of them per unit area and their economic value as well as value of different assets in the flooding area is obtained from a field survey and interviews with the local authorities and local inhabitants, and engineering judgment. Table 3 provides details of the physical damages to the land uses for different return periods. Similarly, the increased rainfall due to El-Niño is simulated and the damages are estimated in the same procedure (Table 4). The results show that the relative increase of the expected flood damages during El-Niño event is much higher than that of rainfall increase. Moreover, for the shorter return period floods, the relative increase of flood damages is much higher than that in the longer return period floods. Specifically, for 5-year floods, expected flood damages during El-Niño could increase by 1671%. The main reason for this high relative increase is that the average depth of 5-yr flood is very small (<0.04m). With an increase of 12.2% in the rainfall intensity during El-Niño event, the flood depth increases considerably (about 0.5m). For the 10-yr and 50-yr floods, expected flood damages due to El-Niño would increase by 176% and 52%, respectively.

The high percentage increase of damage for 5-yr floods may be related to the fact that the initial losses and infiltration amounts are considerable large compared to the 5-year rainfall. When rainfall is relatively small, the effective rainfall is reduced due to retention (rainfall not converted into runoff). For large storm with longer return periods, infiltration and initial losses is small compared to the rainfall. Therefore, the effect of infiltration and initial losses are insignificant, and increase in rainfall intensity will be reflected in the increase in effective precipitation and direct runoff for floods with long return periods.

5 Conclusions

In this paper, the effect of El-Niño on the flood damages was investigated. The methodology was based on the calculation of increasing rainfall amount during El-Niño event compared to the normal conditions. Considering SOI=-1.0 as the threshold of El-Niño, the annual %-increased rainfall is 12.2%. It should be noted that the annual change factor may not necessarily be transferred to extreme values. Nonetheless, the annual change factor was applied for generating design storms of different return periods of 5, 10 and 50 years. Using the HEC-HMS hydrologic model and HEC-RAS hydraulic model, the flood inundation area was simulated for both episodes of neutral and El-Niño. A total of 6 model runs were implemented and flood damages were assessed based on the simulated flood inundation and depth maps. The damage-depth curve method was used to estimate the flood damages. The results showed that the relative increase of expected damage under El-Niño condition is much higher for short return period floods than that for long return period floods. More specifically, in a flood with a return period of 5 years, El-Niño would lead to an increase of 1671% in damages. The relative change in the expected damage is 176% for 10-yr return period flood, while it is 52% for 50-yr return period flood. It suggests that flood managers should pay more attentions to small floods during El-Niño years. The flood management for small but frequent flood requires much less financial budget and may result in much more effective approaches. The results provide decision makers with essential information on flood risk and highlight the importance to take in to account the probable effect of El-Niño in flood risk management.

Acknowledgments

This research is partially supported by the National Natural Science Foundation of China (41730645, 41790424, 41425002), the Strategic Priority Research Program of the Chinese Academy of Sciences (XDA20060402), and the International Partnership Program of Chinese Academy of Sciences (131A11KYSB20170113). Qiuhong Tang is supported by the Newton Advanced Fellowship.

Conflict of interest

The authors declare no conflict of interest.

References

Australia Bureau of Meteorology: Record-breaking La Niña events. An analysis of the La Niña life cycle and the impacts and significance of the 2010–11 and 2011–12 La Niña events in Australia, Bureau of Meteorology, http://www.bom.gov.au/climate/enso/history/ln-2010-12/, 2012.

Alizadeh-Choobari, O. and Najafi, M.S.: Climate variability in Iran in response to the diversity of the El Niño- Southern Oscillation. International Journal of Climatology, 38(11), 4239-4250, https://doi.org/10.1002/joc.5564, 2017.

Azmoodehfar, M.H. and Azarmsa, S.A.: Assessment the effect of ENSO on weather temperature changes using fuzzy analysis (Case study: Chabahar). APCBEE Procedia 5, 508-513, https://doi.org/10.1016/j.apcbee.2013.05.086, 2013.

Berkman, M.P. and Brown, T.: Estimating flood impacts: A status report. In: Australasian Coasts & Ports Conference 2015: 22nd Australasian Coastal and Ocean Engineering Conference and the 15th Australasian Port and Harbour Conference (p. 114). Engineers Australia and IPENZ. https://search.informit.com.au/documentSummary;dn=703231098671457;res=IELIAC, 2015.

Changnon, S.: Measures of economic impacts of weather extremes. Bulletin of the American Meteorological Society, 84, 1231–1235, https://doi.org/10.1175/BAMS-84-9-1231, 2015, 2003.

Corringham, T.W. and Cayan, D.R.: The effect of El Niño on flood damages in the western United States, Weather, Climate, and Society, 11(3), 489-504. https://doi.org/10.1175/WCAS-D-18-0071.1, 2019.

Corry, M., Jones, J. and Thompson, D.: The design of encroachments of floodplains using risk analysis, Hydraulic Engineering Circular, No. 17, Department of Transportation, Federal Highway Administration, Washington, DC, 1980.

Cover, T.M. and Thomas, J.A.: Elements of Information Theory (Wiley ed.). ISBN 978-0-471-24195-9, 1991.

Gholizadeh, M.H.: Evaluation of relation between rainfall and El Niño phenomena in Iran, International Research Journal, 5(1), 1-11, https://irj.iars.info/volumes/828005012015/pdf/828005012015O1.pdf, 2015.

Guiasu, S.: Information Theory with Applications. McGraw-Hill, New York. ISBN 978-0-07-025109-0, 1977.

Grieco, M.B. and DeGaetano, A.T.: A climatology of extreme wave height events impacting eastern Lake Ontario shorelines. Theoretical and Applied Climatology, https://doi.org/10.1007/s00704-018-2502-9, 1-10, 2018.

Hagh-Negahdar, A., Saghafian, B. and Aktari, R.: Investigating the influence of the El Niño - South Oscillation on the annual maximum floods in the southwest of Iran. Journal of Water and Wastewater, 64-78, http://www.wwjournal.ir/article_2160.html, 2007 (In Persian).

Hao, Z., Hao, F., Singh, V.P., Zhang, X.: Quantifying the relationship between compound dry and hot events and El Niño–Southern Oscillation (ENSO) at the global scale, Journal of Hydrology, doi: https://doi.org/10.1016/j.jhydrol.2018.10.022, 2018.

Hooshyaripor, F., Faraji-Ashkavar, S., Koohyian, F. and Dehghani, M.: Estimation of the Effect of Large-Scale Signals on Regional Rainfall of Iran by Statistical Analysis. Asas Journal, 20 (53), 65-76, http://www.isceiran.org/article_90975_en.html, 2019 (In Persian).

Hooshyaripor, F., Tahershamsi, A. and Razi, S.: Dam break flood wave under different reservoir's capacities and lengths, Sādhanā, 42(9), 1557-1569, https://doi.org/10.1007/s12046-017-0693-x, 2017.

Hooshyaripor, F. and Yazdi, J.: A new methodology for surcharge risk management in urban areas (case study: Gonbad-e-Kavus city). Water Science and Technology, 75(4), 823-832, https://doi.org/10.2166/wst.2016.567, 2017.

https://www.farsnews.com/news/13940704000378.

https://www.isna.ir/news/94042914923.

http://www.cpc.ncep.noaa.gov/data/indices/soi.

Jamali, B., Löwe, R., Bach, P.M., Urich, C., Arnbjerg-Nielsen, K., Deletic, A.: A rapid urban flood inundation and damage assessment model, Journal of Hydrology, 564, 1085-1098, https://doi.org/10.1016/ j.jhydrol.2018.07.064, 2018.

KGS_Group: Red River Basin-stage-damage curves update and preparation of flood damage maps, Report prepared for international joint commission, Winnipeg, Manitoba, Canada, https://doi.org/10.1061/40517(2000)118, 2000.

Messner, F., Penning-Rowsell, E., Green, C., Meyer, V., Tunstall, S. and Veen, D.: Evaluating flood damages: guidance and recommendations on principles and models, Sixth framework programme for European research and technological development, integrated project flood site, Document Reference T09-06-01, http://www.floodsite.net/html/partner_area/project_docs/T09_06_01_Flood_damage_guidelines_d9_1_v2_2_p44.pdf, 2007.

Noori, R., Karbassi, A.R., Moghaddamnia, A., Han, D., Zokaei-Ashtiani, M.H., Farokhnia, A. and Gousheh, M.G.: Assessment of input variables determination on the SVM model performance using PCA, Gamma test, and forward selection techniques for monthly stream flow prediction. Journal of Hydrology, 401(3-4), 177-189, https://doi.org/10.1016/j.jhydrol.2011.02.021.

Null, J.: El Niño and La Niña: Their relationship to california flood damage, Golden Gate Weather Services, August 2014.

Olesen, L., Löwe, R., Arnbjerg-Nielsen, K.: Flood Damage Assessment Literature Review and Recommended Procedure, Cooperative Research Centre for Water Sensitive Cities, Melbourne, Australia, https://backend.orbit.dtu.dk/ws/portalfiles/portal/130797720/IN_PC956_B4_1_Flood_Damage_web.pdf, 2017.

Ponce, V. and Hawkins, R.: Runoff curve number: Has it reached maturity, Journal of Hydrologic Engineering, 1, 11-19, https://doi.org/10.1061/(ASCE)1084-0699(1996)1:1(11), 1996.

Saghafian, B., Haghnegahdar, A. and Dehghani, M.: Effect of ENSO on annual maximum floods and volume over threshold in the southwestern region of Iran, Hydrological Sciences Journal 62(7), 1039-1049, https://doi.org/10.1080/02626667.2017.1296229, 2017.

Schöngart, J. and Junk, W.J.: Forecasting the flood-pulse in Central Amazonia by ENSO-indices. Journal of Hydrology 335(1), 124-132, https://doi.org/10.1016/j.jhydrol.2006.11.005, 2007.

Sturges, H.: The choice of a class-interval. J. Amer. Statist. Assoc., 21, 65-66, 1926.

Sun, X., Renard, B., Thyer, M., Westra, S. and Lang, M.: A global analysis of the asymmetric effect of ENSO on extreme precipitation, Journal of Hydrology 530, 51-65, https://doi.org/10.1016/j.jhydrol.2015.09.016, 2015.

Tang, Q.: Global change hydrology: Terrestrial water cycle and global change, Science China Earth Sciences, 63, 459-462, https://doi.org/10.1007/s11430-019-9559-9, 2020.

Wang, Y., Zhang, X., Tang, Q., Mu, M., Zhang, C., Lv, A., Jia, S.: Assessing flood risk in Baiyangdian Lake area in a changing climate using an integrated hydrological-hydrodynamic modelling, Hydrological Sciences Journal, 64(16), 2006-2014, https://doi.org/10.1080/02626667.2019.1657577, 2019.

Ward, P.J., Eisner, S., Florke, M., Dettinger, M.D. and Kummu, M.: Annual flood sensitivities to El-Niño-Southern Oscillation at the global scale, Hydrology and Earth System Sciences, 18, 47-66, https://doi.org/10.5194/hess-18-47-2014, 2014.

Ward, P.J., Jongman, B., Kummu, M., Dettinger, M.D., Sperna Weiland, F.C. and Winsemius, H.C.: Strong influence of El Niño Southern Oscillation on flood risk around the world, Proceeding of National Academy of Sciences of America (PNAS), 111(44), 15659-15664, https://doi.org/10.1073/pnas.1409822111, 2014.

Ward P.J., Kummu M., and Lall U.: Flood frequencies and durations and their response to El Niño Southern Oscillation: Global analysis, Journal of Hydrology, 539, 358-378, https://doi.org/10.1016/j.jhydrol.2016.05.045, 2016.

WRCC (Western Regional Climate Center): Understanding El Niño for your fire management unit, https://wrcc.dri.edu/, January 2010.

Wobus, C., Gutmann, E., Jones, R., Rissing, M., Mizukami, N., Lorie, M., Mahoney, H., Wood, A. W., Mills, D., and Martinich, J.: Climate change impacts on flood risk and asset damages within mapped 100-year floodplains of the contiguous United States, Natural Hazards and Earth System Sciences, 17, 2199-2211, https://doi.org/10.5194/nhess-17-2199-2017, 2017.

WRI (Water Research Institute): Integrated flood management, case study: Kan basin, Report of hydraulic modeling and flood zoning, Water Research Institute, Ministry of Energy, Iran, 2011a.

WRI (Water Research Institute): Integrated flood management, case study: Kan basin, Report of Hydrologic Study and Flood, Water Research Institute, Ministry of Energy, Iran, 2011b.

WRI (Water Research Institute): Integrated flood management, case study: Kan basin. Report of flood vulnerability assessment, Water Research Institute, Ministry of Energy, Iran, 2011c.

Yazdi, J. and Salehi Neyshabouri, S.A.A.: Optimal design of flood-control multi-reservoir system on a watershed scale, Natural Hazards 63(2), 629-646, https://doi.org/10.1007/s11069-012-0169-6, 2012.

Yazdi, J., Salehi Neyshabouri, S.A.A., Niksokhan, M.H., Sheshangosht, S. and Elmi, M.: Optimal prioritisation of watershed management measures for flood risk mitigation on a watershed scale, Journal of Flood Risk Management, 6(4), 372-384, https://doi.org/10.1111/jfr3.12016, 2013.

Table Captions:

Table 1 Correlation coefficient (r) and p-value between precipitation at Mehrabad station and different teleconnection indices

Table 2: The calibrated parameters for the HEC-HMS hydrologic model

Table 3: Physical damages to the sub basins properties for flood in different return periods

Table 4: Flood damages and expected increases during El-Niño condition

Figure Captions:

Figure 1: Location of the Kan River Basin in north of Tehran plain, Iran

Figure 2: Damage-depth curves for different land uses of a) Building and its contents, b) Restaurant's content, and c) agriculture in the Kan River Basin.

Figure 3: Annual rainfall against SOI index at the stations of a) Mehrabad, b) Shemiran, c) Chitgar and 4) Tehran Geophysics

Figure 4: The observed and simulated flood hydrographs in a) calibration step at Sulaghan Station (15–18 April 2003); b) calibration step at upstream gauges (15–18 April 2003); and c) verification step at Sulaghan Station(16–19 April 2002, 15–17 April 2009, and 11–13 March 2011)

Figure 5: The 50-yr floodplain in the sub-basins of a) Sulaghan and b) Sangan (The original layers are obtained from WRI 2011a)

Table 1

Index	SOI	MEI	NAO	AO	MJO
r	0.32	0.29	0.15	0.002	0.1
p-value	0.016	0.02	0.029	0.84	0.9

Table 2

No.	Sub-basin	Area (km^2)	Calibrated parameter	
			CN	*Tc* (hr)
1	Imamzadeh Davood	23.77	71.87	1.05
2	Rendan	33.61	72.35	0.874
3	Sangan	47.43	71.37	1.227
4	Taloon	26.65	71.39	0.932
5	Kiga	4.40	70.2	0.332
6	Doab	7.19	71.71	0.511
7	Keshar	34.85	71.83	1.181
8	Herias	11.44	70.7	0.759
9	Sulaghan	13.66	71.1	0.556
10	Jangalak	12.89	71.9	0.623

Table 3

50-yr flood					
Sub-basin	Average inundation depth (m)	Damage to residential building (10^3US$)	Damage to content (10^3US$)	Damage to restaurant (10^3US$)	Damage to agriculture (US$)
Imamzadeh Davood	0.61	201	37	42	519
Rendan	0.6	68	12	20	723
Sangan	0.5	393	68	19	1,259
Keshar	0.66	343	62	67	550
Sulaghan	0.25	81	11	55	843
Sum (10^3US$)		**1,086**	**190**	**203**	**3,893**
Total damage cost (10^3US$)					**5,372**
10-yr flood					
Imamzadeh Davood	0.15	29	3.2	6.1	107
Rendan	0.2	17	2.2	5.1	249
Sangan	0.09	21	6.2	1	210
Keshar	0.41	202	46	39.6	283
Sulaghan	0.05	11	2.3	7.3	145
Sum (10^3US$)		**280**	**60**	**59.1**	**994**
Total damage cost (10^3US$)					**1,394**
5-yr flood					
Imamzadeh Davood	0.03	4.9	0.98	1.02	36
Rendan	0.01	1.4	0.11	0.41	6.2
Sangan	0.009	4.1	0.61	0.2	0
Keshar	0.04	9.3	2.1	1.83	16
Sulaghan	0.01	5.4	0.45	3.66	26
Sum (10^3US$)		**25.1**	**4.2**	**7.12**	**84.2**
Total damage cost (10^3US$)					**121**

5

Table 4

Flood return period (yr)	Damage assessment (US$)		Relative increase in damage (%)
	El-Niño neutral condition	El-Niño condition	
5	120,529	2,135,486	1,671
10	1,393,753	3,852,095	176
50	5,372,472	8,158,454	52

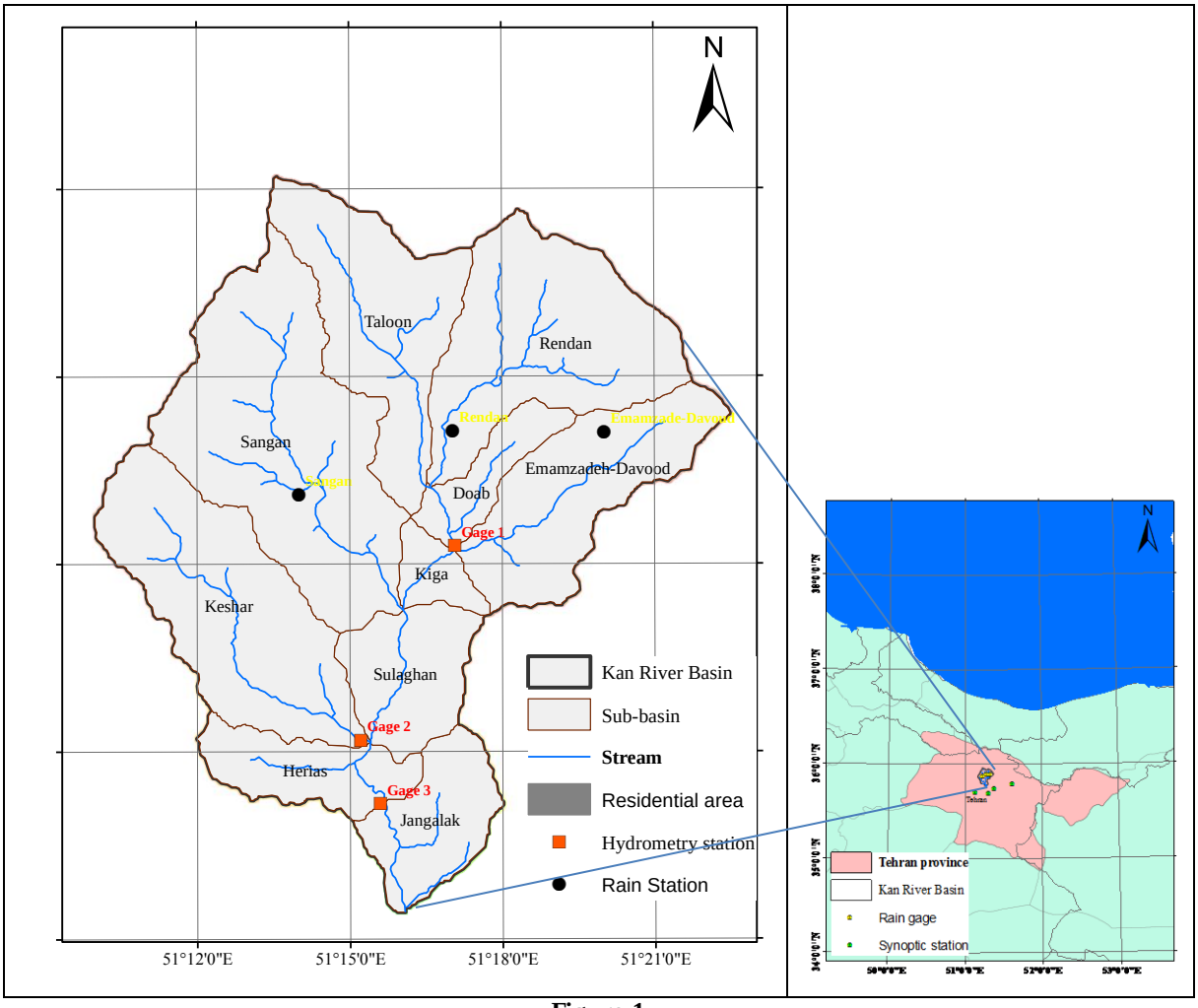
N
Taloon
Rendan
Rendan
Emamzade-Davood
Sangan
Sangan
Emamzadeh-Davood
Doab
Gage 1
Kiga
Keshar
Sulaghan
Gage 2
Herias
Gage 3
Jangalak
Kan River Basin
Sub-basin
Stream
Residential area
Hydrometry station
Rain Station
51°12'0"E
51°15'0"E
51°18'0"E
51°21'0"E
N
Tehran province
Kan River Basin
Rain gage
Synoptic station

Figure 1

5

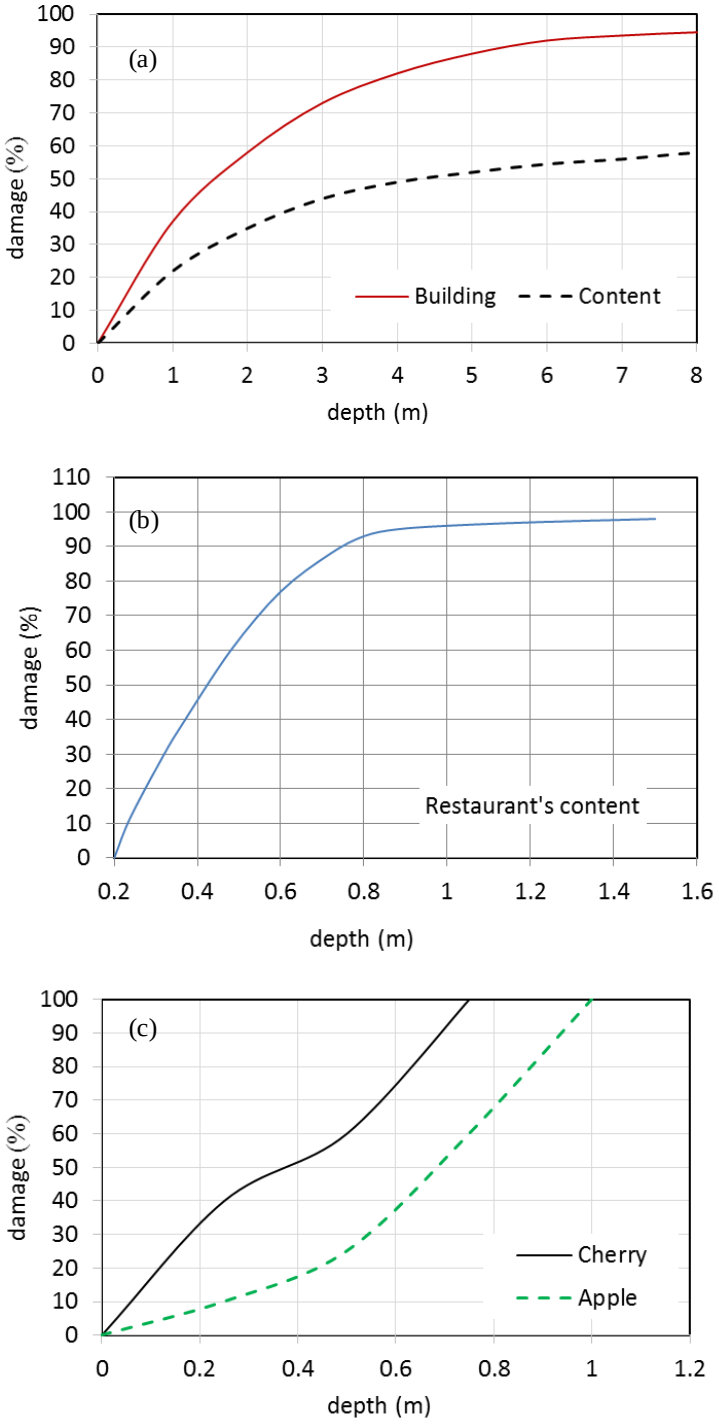
(a)
damage (%)
depth (m)
Building
Content
(b)
damage (%)
depth (m)
Restaurant's content
(c)
damage (%)
depth (m)
Cherry
Apple

Figure 2

5

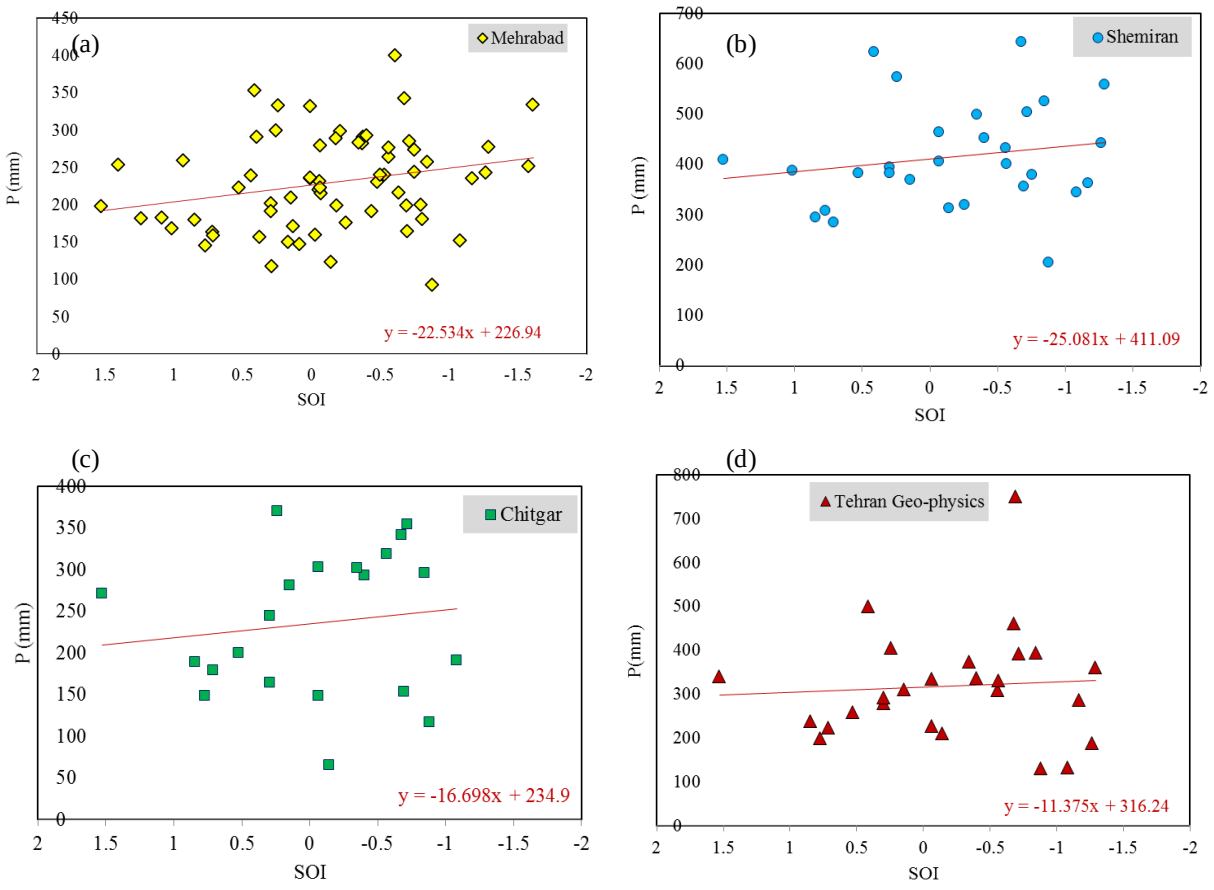
(a)
Mehrabad
P (mm)
SOI
y = -22.534x + 226.94
(b)
Shemiran
P (mm)
SOI
y = -25.081x + 411.09
(c)
Chitgar
P (mm)
SOI
y = -16.698x + 234.9
(d)
Tehran Geo-physics
P(mm)
SOI
y = -11.375x + 316.24

Figure 3

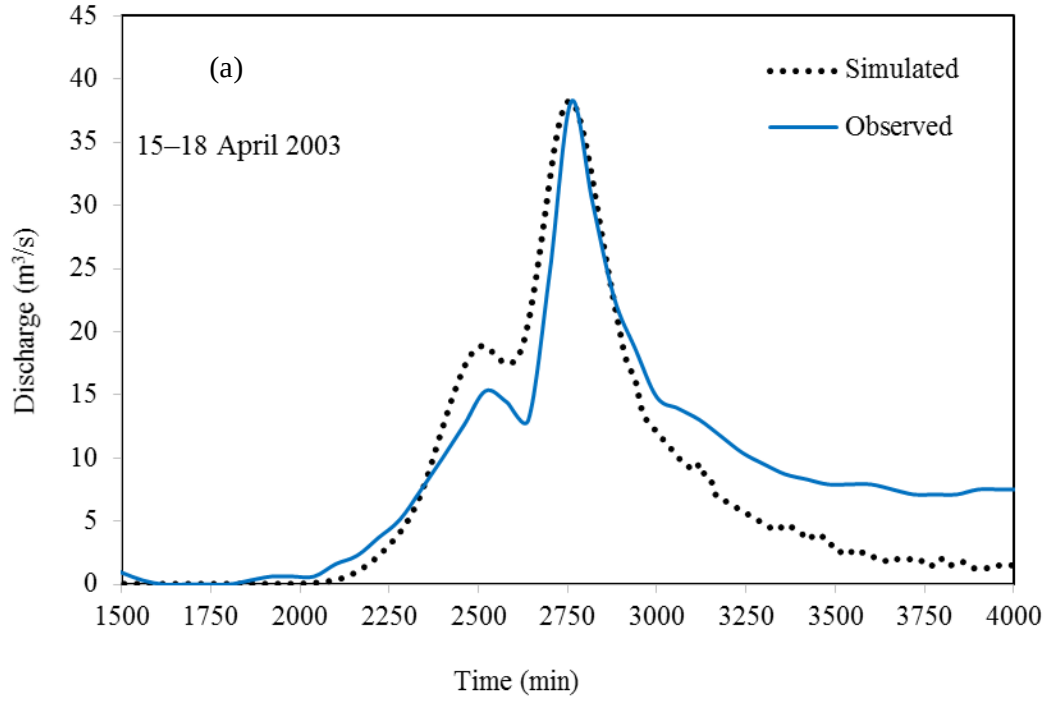
(a)
15–18 April 2003
Simulated
Observed
Discharge (m3/s)
Time (min)
0
5
10
15
20
25
30
35
40
45
1500
1750
2000
2250
2500
2750
3000
3250
3500
3750
4000

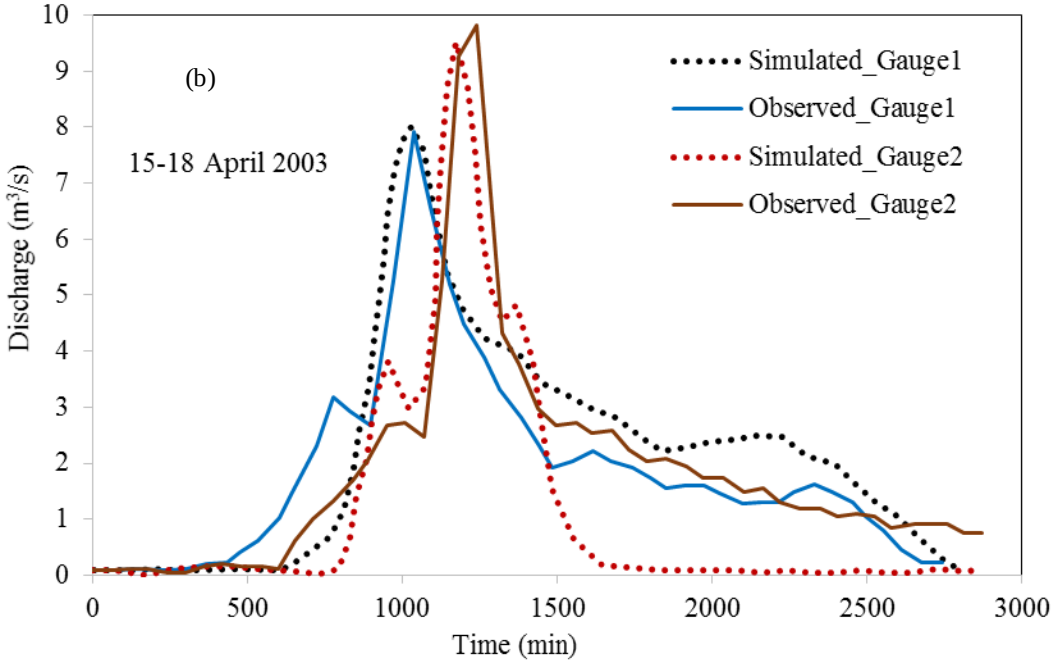
(b)
15-18 April 2003
Simulated_Gauge1
Observed_Gauge1
Simulated_Gauge2
Observed_Gauge2
Discharge (m3/s)
Time (min)
0
1
2
3
4
5
6
7
8
9
10
0
500
1000
1500
2000
2500
3000

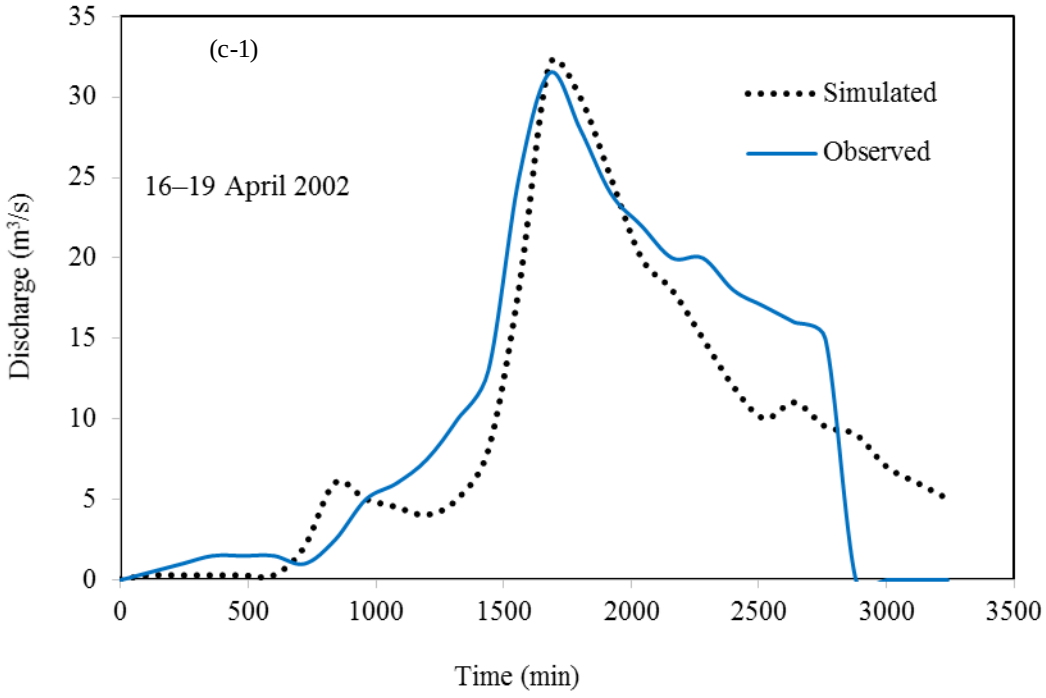
(c-1)
16–19 April 2002
Simulated
Observed
Discharge (m³/s)
Time (min)
0
5
10
15
20
25
30
35
0
500
1000
1500
2000
2500
3000
3500

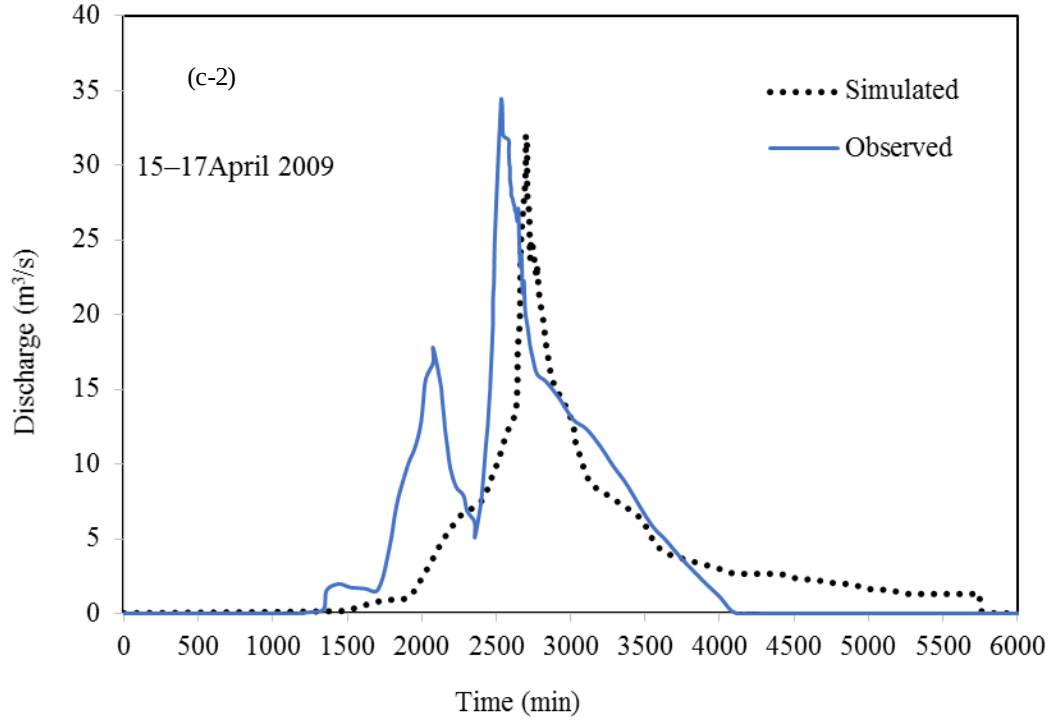
(c-2)
15–17April 2009
Simulated
Observed
Discharge (m³/s)
Time (min)
0
5
10
15
20
25
30
35
40
0
500
1000
1500
2000
2500
3000
3500
4000
4500
5000
5500
6000

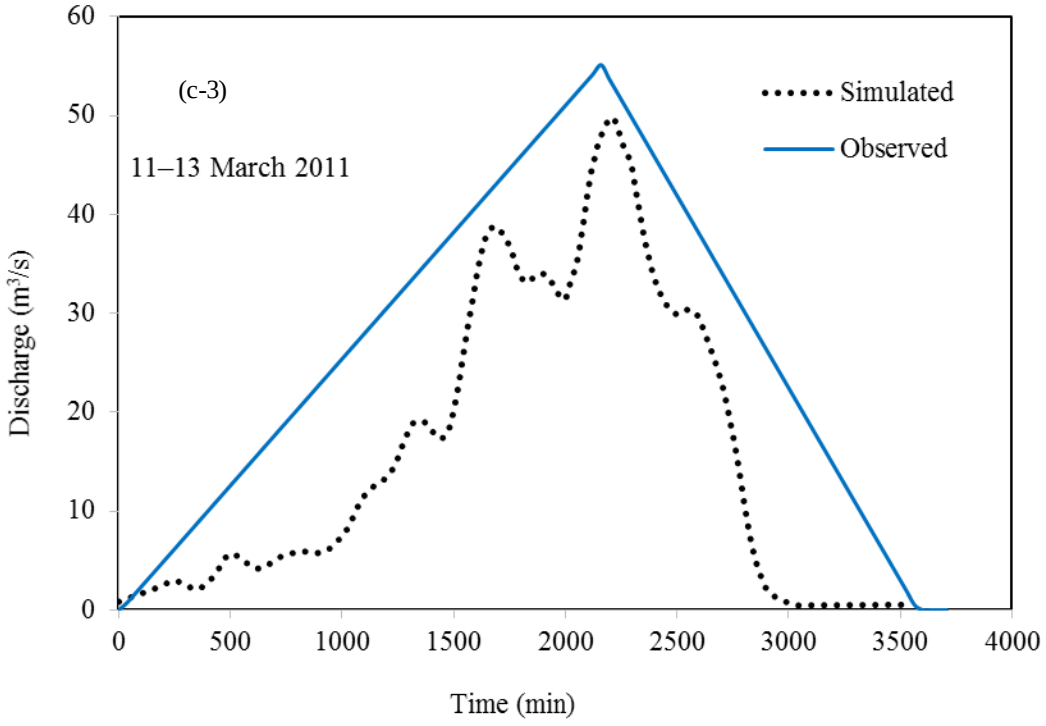
(c-3)
11–13 March 2011
Simulated
Observed
Discharge (m³/s)
Time (min)
0
10
20
30
40
50
60
0
500
1000
1500
2000
2500
3000
3500
4000

Figure 4

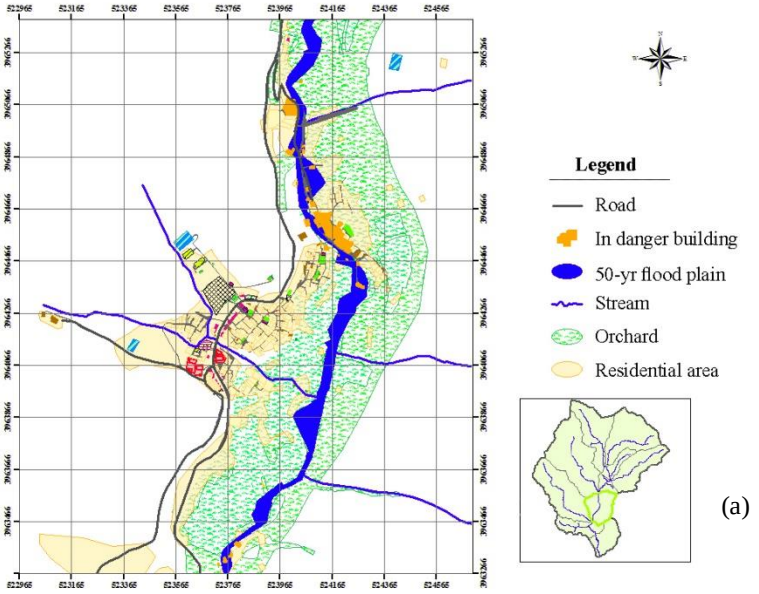
Legend
Road
In danger building
50-yr flood plain
Stream
Orchard
Residential area

(a)

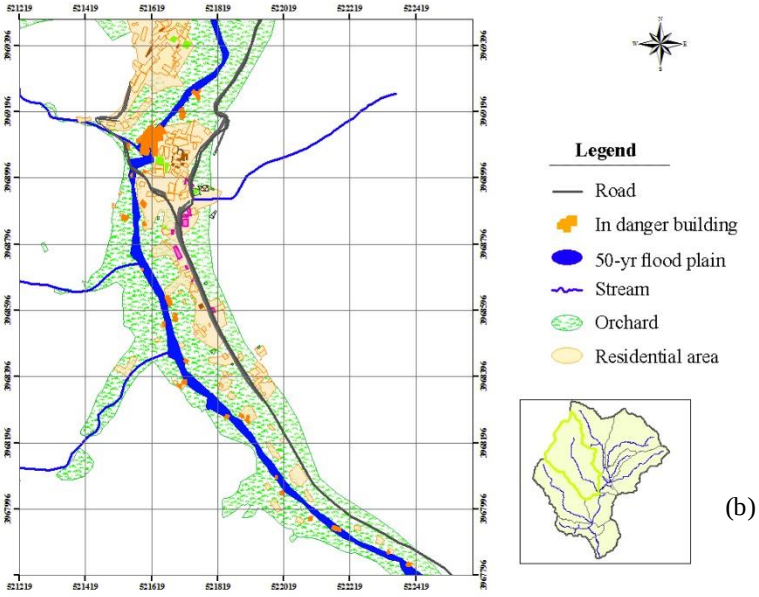
Legend
Road
In danger building
50-yr flood plain
Stream
Orchard
Residential area

(b)

Figure 5